Quantum Electronics **48** (9) 826–832 (2018)

INTERACTION OF LASER RADIATION WITH MATTER. LASER PLASMA https://doi.org/10.1070/QEL16693

Temporal dynamics of air plasma glow under different focusing conditions of a femtosecond radiation pulse

N.G. Ivanov, V.F. Losev, V.E. Prokop'ev

Abstract. **We report the results of the spectral and temporal investigations of air plasma glow with a temporal resolution of ~2 ps. The plasma was produced by 950-nm laser pulses 60 fs in duration. It is shown that the spectrum obtained for a numerical aperture NA > 0.1 is dominated by atomic and ionic lines of oxygen and nitrogen against the background of a high-intensity continuous spectrum in the visible region. For NA < 0.07, the lines of the second positive system of molecular nitrogen N_2 and the first negative system of N_2^+ molecular ions make their appearance in the spectrum. For NA < 0.03, the spectrum consists only of the molecular lines of N_2 and N_2^+. The emission intensity peaks of these lines lag behind the laser pulse by 10–12 ps, but the atomic lines begin to shine 80–100 ps after the instant of irradiation. The characteristic time of line glow decay to a 1/e level amounts to 18 ps for N_2^+, to 27 ps for N_2, and to 20 ns for atomic lines.**

Keywords: *femtosecond laser radiation, focusing in the air, numerical aperture, molecular and atomic emission lines, radiation pulse duration, second harmonic, spectral line, plasma radiation.*

1. Introduction

The temporal glow dynamics of the plasma produced by a femtosecond radiation pulse was first studied in Ref. [1]. To produce the filament plasma, use was made of neodymium laser radiation with a wavelength of 1.053 μm and a pulse duration of 500 fs. The spectra were recorded with a time-gated spectrometer (the shortest width of 4.5 ns) and a streak camera (without spectral resolution). Three stages of plasma glow were revealed. Prevailing at the first stage are the molecular lines of N_2 and N_2^+ (the 2^+ system of N_2 dominates), which manifest themselves immediately after the laser irradiation (the time t_0) with a characteristic decay time $\tau \approx 60$ ps. A continuous spectrum with $\tau \approx 30$ ns becomes prevalent at the second stage, 1 ns after t_0. As it decays, at the third stage, atomic lines of oxygen and nitrogen begin to show up, which shine during $\tau \approx 1$ μs. In Ref. [2], the duration of N_2 glow in the filament was measured at ~85 ps by pump–probe technique. At the same time, in Ref. [3] the duration of only the rise time of the N_2^+ and N_2 glow was measured at 150–200 ps. However, it is pertinent to note that the minimal signal exposure time was equal to 100 ps. Recent measurements [4] by a streak camera with a high time resolution (30 ps) showed that the N_2^+ glow rise time was determined by the time resolution and that $\tau = 600$ ps. The authors of this work associate the value of τ with the free-electron lifetime in the plasma and believe that it is determined by the electron quenching of the upper state of N_2^+ ($B^2\Sigma_u^+$).

The use of interferometry and the pump–probe technique permits measuring the electron density (N_e) in the filament plasma with a subpicosecond time resolution [5, 6]. As shown in Ref. [6], the electron density depends on the nitrogen pressure and decreases by more than an order of magnitude (from 10^{17} to 6×10^{15} cm^{-3}) during 1 ns at a pressure of 1 atm. At the same time, several papers report that the characteristic density (N_e) decay time is 1–10 ns [7–9].

Therefore, the data on the temporal evolution of the glow characteristics and the electron density of the plasma produced by a femtosecond radiation pulse in the air are rather contradictory and invite further investigation.

Our work was aimed to study the temporal dynamics of the emission spectrum and the electron density of the plasma produced by femtosecond radiation pulses with the use of a streak camera, which provides a temporal resolution of 2 ps. We present data on the dynamics of the emission spectrum and the electron plasma density in the air, and analyse the production mechanisms of excited particles and the kinetics of their quenching.

2. Experiment

2.1. Experimental facility and methods

In our experiments we employed a Ti:sapphire laser system (Avesta Ltd.), which generated laser radiation at a centre wavelength $\lambda = 950$ nm with a pulse duration of 60 fs (FWHM), an energy of up to 15 mJ, and a pulse repetition rate of 10 Hz. The radiation was focused in the atmospheric air using lenses with focal distances $F = 3 - 326$ cm. The pulse-to-pulse energy jitter measured ± 5%. The initial beam had a diameter of 10 mm (at a $1/e^2$ level), a radiation quality factor $M^2 = 1.5$, and a close-to-Gaussian transverse intensity profile. In some experiments the radiation was partly converted to the second harmonic (SH) in a 2-mm thick KDP crystal. The SH fulfilled the function of recording the instant of laser irradiation on the time scale. The experimental facility used to carry out the measurements is schematised in Fig. 1.

The glow dynamics of different plasma components was measured transversely to the filament direction. To this end, two condensers collected the plasma radiation and focused it on the spectrometer slit. After the spectrometer the radiation was directed to the entrance slit of the streak camera. The

N.G. Ivanov, V.F. Losev, V.E. Prokop'ev Institute of High Current Electronics, Siberian Branch, Russian Academy of Sciences, Akademicheskii prosp. 2/3, 634055 Tomsk, Russia; e-mail: losev@ogl.hcei.tsc.ru

Received 4 April 2018; revision received 21 May 2018
Kvantovaya Elektronika **48** (9) 826–832 (2018)
Translated by E.N. Ragozin

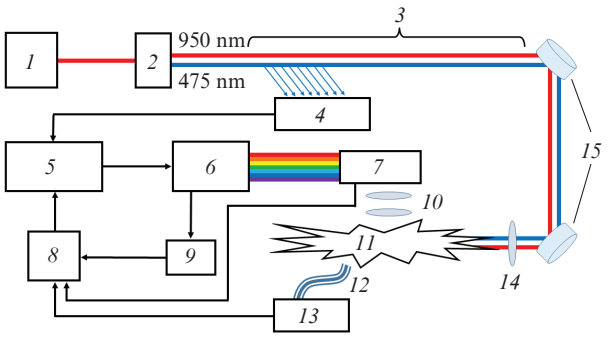

Figure 1. Schematic of the experimental facility: (*1*) Ti:sapphire laser; (*2*) KDP crystal; (*3*) optical delay line; (*4*) PIN diode; (*5*) delay generator; (*6*) streak camera; (*7*) SP-2300; (*8*) PC; (*9*) CCD matrix; (*10*) condensers; (*11*) plasma; (*12*) light guide; (*13*) HR-4000; (*14*) lens; (*15*) mirrors.

time- and spectrum-resolved image at its output was recorded with a CCD matrix. Next the information was transferred to a computer via an interface and processed. The spectrometer (Acton Spectra Pro SP-2300) was equipped with three interchangeable gratings: 50, 300, and 1200 grooves mm^{-1}. The highest spectral resolution for the minimal entrance slit was equal to 0.27 nm. The streak camera (Hamamatsu, Universal Streak Camera C10910) had two time bases: the fast base (the shortest sweep duration of 100 ps) and the slow one (the shortest sweep duration of 1 ns). The highest time resolution of the streak camera was equal to 0.644 ps. In the pulse accumulation regime the time resolution amounted to 4.3 ps for 10000 shots owing to the jitter of streak-camera triggering. To reduce the jitter, in the measurements the camera was triggered with a PIN diode, which recorded the scattered pump radiation and was placed near the spectrometer. The resultant signal from the streak camera was averaged over 300 pulses. To compensate for the retardation time of the sweep unit of the streak camera, the laser radiation traversed a distance of about 14 m and was only then focused. The measurement of plasma channel diameter in time was performed in the scheme, in which the radiation was focused along the spectrometer slit. In this case, the spectrometer was switched to the '0' regime, whereby the spectral resolution was absent. To estimate the electron density, we also studied in our experiments the dynamics of Stark broadening of the hydrogen line H_α. In this case, the fundamental harmonic radiation was focused into a cell filled with a 15:1 nitrogen–hydrogen mixture at a total pressure of 1.5 atm. The time integrated spectra of the filament plasma glow were recorded by an HR-4000 spectrometer (Ocean Optics, 200–1100 nm) with a spectral resolution of 0.75 nm.

2.2. Streak camera calibration

Combining the spectrometer with the streak camera gives rise to an error in the determination of the instant of appearance of different wavelengths. This is caused by the fact that the radiation of different wavelength λ traverses different distances to the streak camera photocathode owing to dispersion. For a sweep duration shorter than 1 ns this error becomes significant. To determine the time delay for the radiation of different wavelength, we performed temporal calibration of the instrument. For a light source, use was made of a highly directional supercontinuum in a broad spectral range (350–1000 nm) [10]. For so broad a spectrum of the supercontinuum and its rather long transportation path, the dispersion of the air might affect the calibration accuracy. However, our estimates showed that the transportation of the radiation with λ = 350 nm (n_{350} = 1.00028973) and 1000 nm (n_{1000} = 1.00027505) through a distance of 14 m gives rise to a time difference $\Delta t = \Delta n \times l/c = 0.685$ ps, where Δn is the difference between the refractive indices n of the air at these wavelengths, l is the path length, and c is the speed of light. Therefore, the dispersion of the air makes a contribution comparable with the time resolution of the instrument. By way of example Fig. 2 shows the picture of lagging of the short-wavelength supercontinuum components from the long-wavelength ones in the range from 350 to 600 nm. One can see that the λ = 375 nm radiation lag from the λ = 600 nm radiation amounts to 5 ps. The calculated time difference for the radiation of different wavelength was taken into account in the recording of the temporal behaviour of plasma glow spectra.

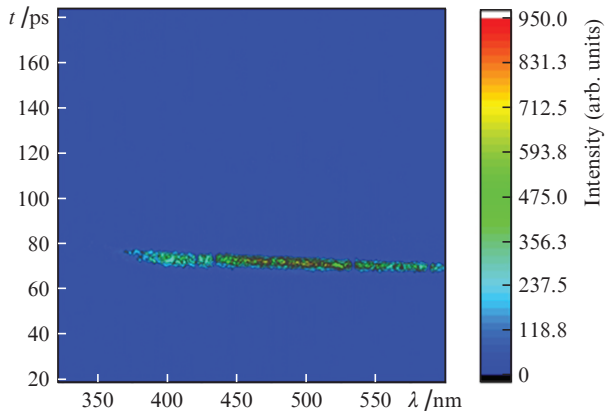

Figure 2. Spectral-temporal image of the glow of directional supercontinuum in the 350–600 nm spectral range.

Prior to the experiments, we also performed the wavelength calibration of the spectral instrument as regards the positions of spectral lines and their intensities with the use of an Hg–Ar lamp and a blackbody radiation source. To determine the limiting time resolution of the streak camera, the SH radiation pulses of 50 fs duration were directed to the spectrometer input in the absence of condensers. In this case, the highest resolution was equal to 2 ps for a 5 μm wide slit of the chronograph and a storage of 300 pulse signals.

3. Experimental results

The shape and glow of the plasma depended heavily on the focal lens distance. Figure 3 shows the photographs of plasma glow and supercontinuum emission in three cases. For a tight focusing (F = 3–10 cm) the glow resembled the emission of an optical breakdown observed in the nanosecond range of radiation pulse duration. In this case, an extremely nonuniform conical supercontinuum was observed behind the plasma object. Its glow changed from pulse to pulse. A longer plasma channel of varying intensity was produced for F = 11–50 cm. The supercontinuum in the form of a bright yellow ring possessed a certain angular directivity, which depended on the pump energy. For F = 100–300 cm, the length of the plasma channel (filament) measured 10–100 cm. For a certain pump

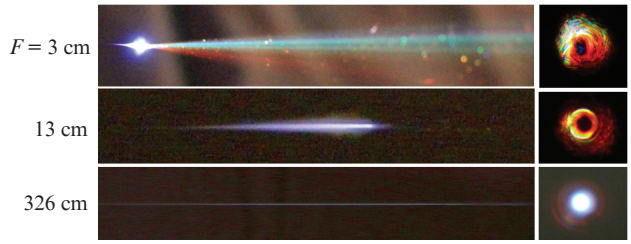

Figure 3. (Colour online) Photographs of the plasma (on the left) and supercontinuum (on the right) glow for different lens focal distances.

energy there appeared an axially directed white supercontinuum behind the filament.

The temporal dynamics of the plasma glow was investigated in the two first cases, since the plasma glow intensity in the third case was too low to be recorded. Figure 4 shows the time-integrated spectrum in the 200–1100 nm range for F = 3 cm. One can see that only atomic and ionic lines of nitrogen, hydrogen, and oxygen are observed in the plasma glow against the continuum background. Figure 5 depicts the dynamics of the atomic glow development in this case. As is seen in the inset, the glow onset is delayed by 87 ps relative to the

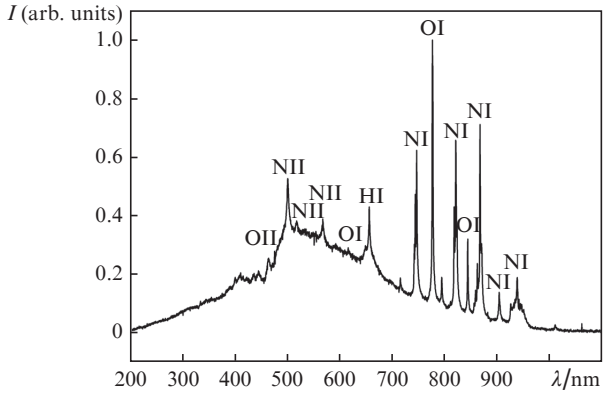

Figure 4. Spectral composition of the plasma radiation for F = 3 cm and E = 15 mJ.

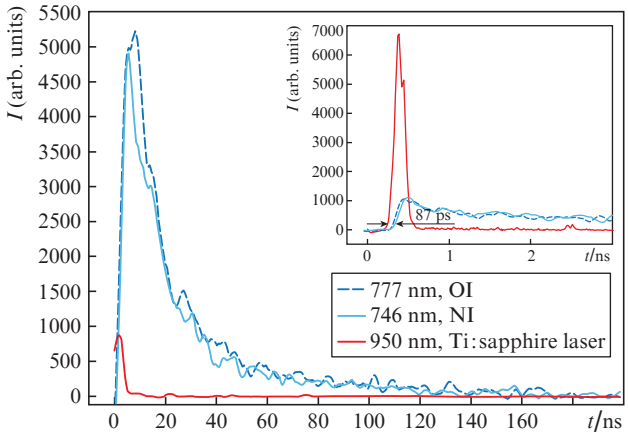

Figure 5. Temporal shapes of the radiation of the atomic lines of nitrogen and oxygen at 746 and 777 nm, respectively, and of the laser radiation at 950 nm; F = 3 cm, the sweep durations are equal to 200 ns and 5 ns (in the inset).

onset of the laser pulse. A similar delay was also observed in Ref. [3]. The intensity peaks ~0.2 ns after the glow onset. The glow intensity decay time at a level of 1/e is equal to 20 ns. The intensities of continuum and of atomic and ionic lines decrease sharply with increasing lens focal distance. In this case, the lines of the 2^+ system of molecular nitrogen N_2 and the 1^- system of the N_2^+ ions begin to manifest themselves clearly in the short-wavelength part of the spectrum. The integral spectrum recorded for F = 20 cm and a pump energy of 8 mJ is presented in Fig. 6, 7. Attention is drawn to the fact that the ion glow duration is much shorter that the glow duration of neutral molecules. For instance, for N_2 molecules the duration $\tau \approx 150$ ps, while for N_2^+ ions $\tau \leqslant 50$ ps. The real duration may be appreciably shorter, because the time resolution for this sweep is not high enough. Attempts to record the plasma

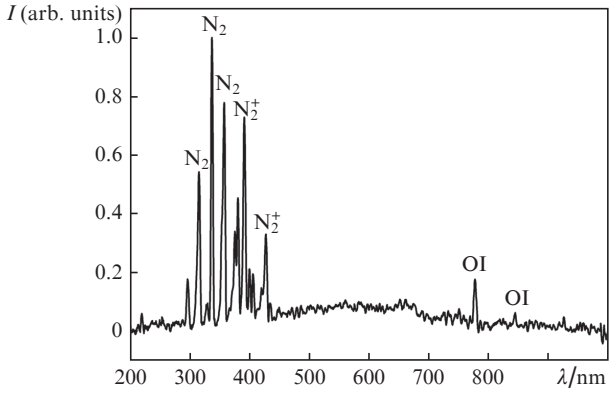

Figure 6. Spectral composition of the plasma radiation for F = 20 cm and E = 8 mJ.

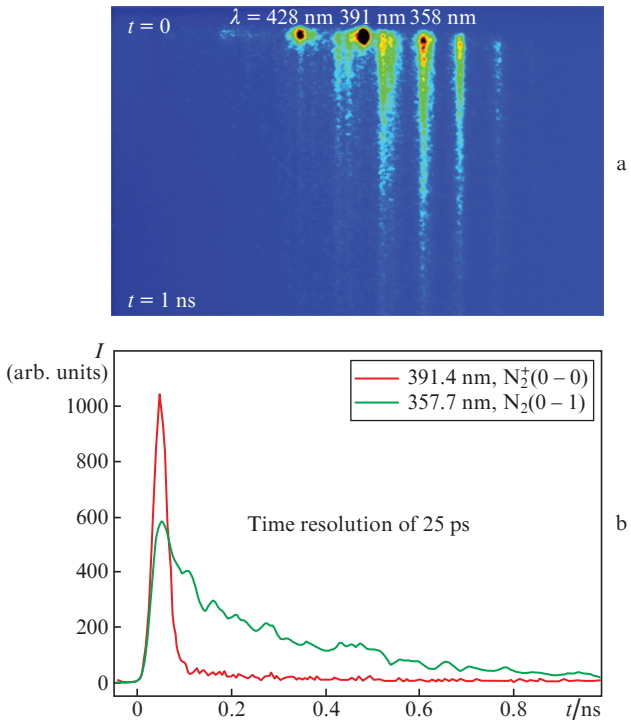

Figure 7. (a) Spectral streak picture of the emission recorded in the range 250–530 nm and (b) temporal radiation behaviour for N_2^+ and N_2; E = 13 mJ, F = 32 cm, the sweep duration is equal to 1 ns.

spectrum under these conditions with the use of the fastest sweep (100 ps) did not meet with success because of the high jitter in the triggering of the streak camera. However, it was possible to record a stable signal using a sweep of 200 ps duration. In this case, we used the procedure of rejecting some photographs. Figure 8 shows the results of processing the spectral-temporal picture of the N_2 and N_2^+ line glow in the plasma.

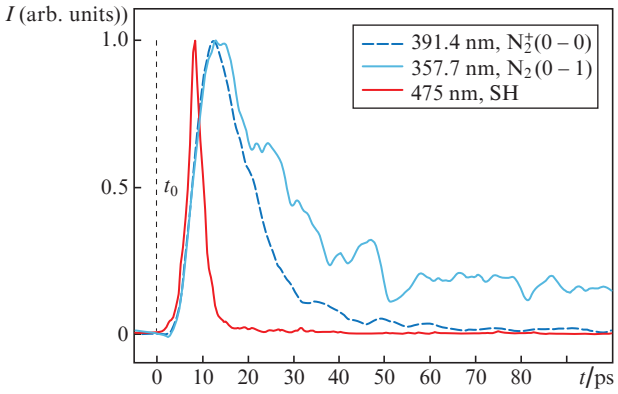

Figure 8. Time dependences of the radiation intensities of the SH, N_2^+, and N_2; the sweep duration is equal to 200 ps.

The pulse shape of the SH with $\lambda = 475$ nm defines the transient characteristic and the time resolution of the instrument under concrete recording conditions. To within this accuracy it may be said that the glow peaks of N_2 molecules and N_2^+ ions lag behind the laser pulse. The N_2^+ ion glow duration amounts to ~ 18 ps at a level of 1/e and to ~ 13 ps at a level of 0.5. The half-amplitude glow duration of N_2 molecules is also short (~ 20 ps).

An analysis of the above data brings up the question: what processes are responsible for so short a lifetime of the upper states of N_2^+ and N_2? It is well known that the radiative lifetime amounts to 60 ns for N_2^+ and to 30 ns for N_2 [1, 11], and so their spontaneous decay cannot determine the lifetimes observed in our work. Collisions with neutral particles may be another quenching process. However, our measurements showed that the N_2^+ and N_2 glow duration is independent of the nitrogen pressure in the 0.1–3 arm range. The same was observed in Ref. [4], though at a low N_2 pressure (~ 8 Torr). Furthermore, in Ref. [1] it was shown that the characteristic lifetime of the $B^2\Sigma_u^+$ state amounts to ~ 60 ps at atmospheric pressure, which is more than three times longer than our measured figure. The authors of Ref. [4] arrived at a conclusion that that the $B^2\Sigma_u^+$ state lifetime is determined by the electron–N_2^+ collision frequency. To estimate how likely it is in our case, we measured the plasma electron density from the broadening of the H_α hydrogen line ($\lambda = 656.3$ nm) [12] at different points in time. Figure 9 shows the time dependence of the hydrogen line broadening and the calculated electron density values.

The electron density was calculated under the assumptions of Stark line broadening and local thermodynamic equilibrium (LTE). According to Ref. [7], this assumption is admissible in our conditions. The presence of continuum in the vicinity of the $\lambda = 656.3$ nm line limited the accuracy of measurements at the initial points in time (up to 50 ps). To improve the accuracy, an approximation curve is plotted in

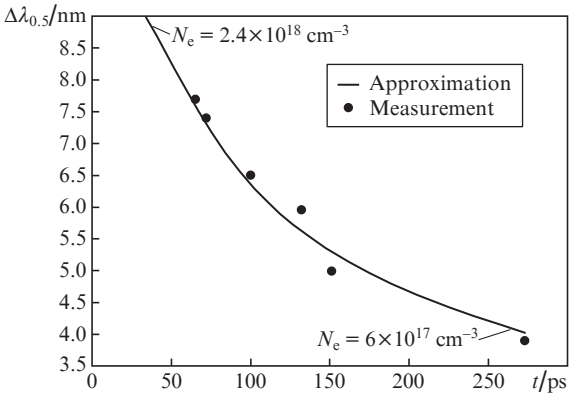

Figure 9. Time dependence of the spectral width of the H_α hydrogen line; $F = 15$ cm, $E = 15$ mJ. The time $t = 0$ ps corresponds to the instant of laser irradiation, $\Delta\lambda_A = 0.65$ nm is the spectral resolution of the instrument.

the drawing. As is seen in Fig. 9, during the first 100 ps there occurs a rapid lowering of the electron density, which subsequently slows down.

Additionally we estimated the electron density proceeding from the intensity of plasma radiation. To estimate the diameter of the beam waist and then the intensity, we measured the diameter of the plasma channel and the variation of its glow intensity with time. In these experiments, the focal lens distance was equal to 6.5 cm and the pulse energy was 3 mJ. Figure 10 shows the results of processing the spatiotemporal recording.

One can see from Fig. 10a that the normalised distribution of the plasma channel radiation intensity remains invari-

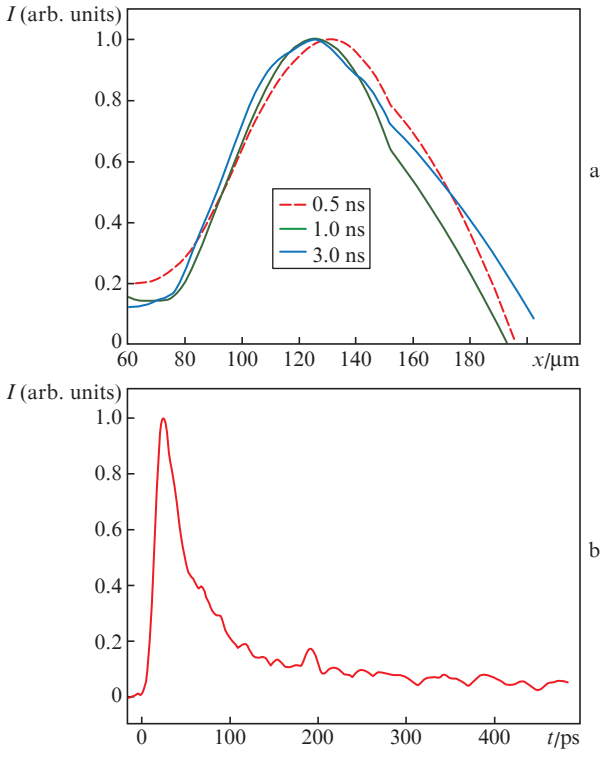

Figure 10. (a) Transverse distributions of plasma radiation intensity and (b) time dependence of the on-axis radiation intensity.

able throughout the time period 0.5–3 ns and that its diameter is ~120 μm. From the relation $d_{pl} = d_{waist}/K^{1/2}$, where K = 9.6 [1] is the Keldysh coefficient and d_{pl} and d_{waist} are the respective diameters of the channel and the waist, we find the waist diameter: $d_{waist} = 0.12 \times 3.1 = 0.37$ mm. The peak radiation intensity in the waist plane for such this size and an energy of 3 mJ amounts to $I_0 \approx 10^{14}$ W cm^{-2}. According to Ref. [13], which studied the dependence of the electron density N_e on the intensity I_0, for $I_0 = 10^{14}$ W cm^{-2} the density $N_e = 10^{18}$ cm^{-3}, which is close to the figure obtained from our measurements of the Stark broadening of the H_α line. Furthermore, a plasma electron density of ~10^{18} cm^{-3} was obtained also in Ref. [14] under conditions similar to ours. As is seen in Fig. 10b, on the plasma channel axis the radiation intensity decay to a level of 0.5 amounts to 34 ps and to a level of 1/e to 60 ps. Proceeding from so short a decay time, one may conclude that the lines of N_2^+ ions and N_2 molecules main the main contribution to the plasma glow under these conditions (see Fig. 7b).

4. Discussion of results

The variation of the spatial and spectral-temporal plasma parameters under NA variation is due to the difference in radiation energy input to the plasma. For large NA (short-focus focusing) the nonlinear and geometrical foci are close to each other. As a result, nearly all radiation passes through the plasma, which increases the absorbed energy fraction. This gives rise to a higher electron density and increases the rate of exchange processes with participation of electrons, the rate of dissociative recombination of molecular ions in particular. Therefore, the radiation arising from the $B^2\Sigma_u^+ - X^2\Sigma_g^+$ transition may not be observed. If it is assumed that N_2 in the state $C^3\Pi_u$ is produced via the dissociative recombination of N_4^+ [2], the radiation of the second positive system of nitrogen would be absent, too. By contrast, the production probability of atomic and ionic excited states becomes high in this case.

For small NA (long-focus focusing) the geometrical factor plays a minor role. The Kerr effect comes into play far ahead of the geometrical focus and the nonlinear phase accumulation takes effect. As a result, in the central part of the beam there appears a high gradient of the phase distribution with a large on-axis phase lag. This increases the on-axis intensity and gives rise to plasma production. On further propagation of the radiation, the phase gradient changes the sign, which limits the inflow of energy from the periphery and lowers the on-axis intensity [15]. This is also fostered by the resultant plasma. Therefore, for small NA there exists a mechanism which impedes the unlimited growth of radiation intensity. The low intensity and the consequential low electron density will serve to lengthen the lifetimes of the excited states and enhance the glow of N_2^+ and N_2.

As is clear from Fig. 8, the radiation pulses of molecules and molecular ions of nitrogen are rather short unlike the pulses described in other works. In this case, the N_2^+ and N_2 glow intensity peaks of lag behind the laser pulse, which testifies to the population of excited levels after laser irradiation. Since the radiation pulse shape is defined by the rates of the mechanisms responsible for the production and quenching of excited particles, we analyse the most important of them.

We begin with an analysis of ion production mechanisms. Figure 11 shows the potential curves of N_2 and N_2^+ as well as the production probability of N_2 autoionising states in relation to exciting photon energy [16]. The lifetimes of autoionising states are extremely short: 10^{-13}–10^{-14} s. Their decay gives rise to an ion and an electron, which carries away the energy defect. As is clear from the inset in Fig. 11, the auotionisation level $3\sigma_g$ of energy 15.58 eV possesses the highest production probability. This level is at perfect resonance with the ground state $X^2\Sigma_g^+$ ($v'' = 0$) of N_2^+ ions. At the same time, the energy of 12 photons with λ = 950 nm amounts to 15.66 eV, and the population probability of the $X^2\Sigma_g^+$ ($v'' = 0$) level via the autoionising state $3\sigma_g$ is therefore very high. The interaction of ions in the $X^2\Sigma_g^+$ ($v'' = 0$) state with three pump photons may give rise to the population of the vibrational–rotational levels of the $B^2\Sigma_u^+$ state with $v' = 3$, since the energy of these three photons is at resonance with the $X^2\Sigma_g^+$ ($v'' = 0$) – $B^2\Sigma_u^+$ ($v' = 3$) transition. When the pump intensity is high enough, there appears a possibility of direct population of the $B^2\Sigma_u^+$ ($v' = 3$) state by 15 photons. Our observed radiation with λ = 391.4 and 427.8 nm nevertheless corresponds to the transitions from the upper state $B^2\Sigma_u^+$ with zero vibrational number. It is well known that the fastest vibrational relaxation of ions is possible in the course of Coulomb collisions with electrons (a so-called e–V relaxation). The rate of this process was theoretically studied in Ref. [17], where the vibrational energy exchange was calculated with the inclusion of autoionising state production via the following reaction chain:

$$N_2^+(v_i^+) + e^-(\varepsilon) \rightarrow N_2^*,\ N_2^{**} \rightarrow N_2^+(v_j^+) + e^-(\varepsilon'). \qquad (1)$$

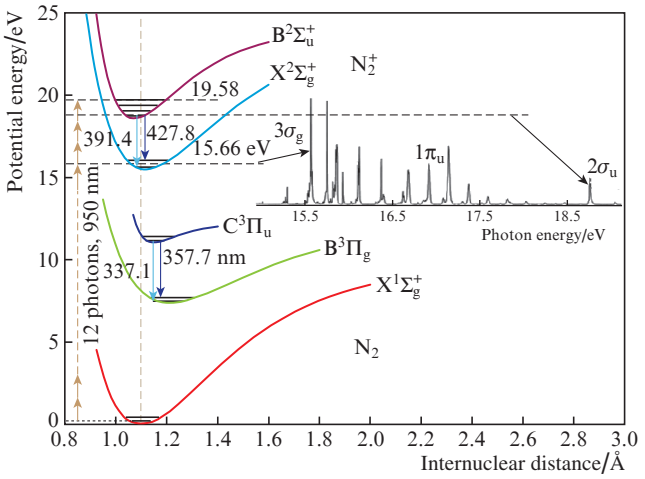

Figure 11. Potential curves of nitrogen as well as observable transitions. The inset shows the autoionising states of N_2 molecules.

Figure 12 depicts the calculated vibrational-energy quenching rate, beginning with level $v'' = 3$ of the ground state of N_2^+ in the electron temperature (T_e) range 100–10000 K (~0.01–1 eV) [17]. If it is assumed that in our conditions $T_e \approx 5000$ K [7], according to calculations the rate coefficient for the e–V relaxation from $v'' = 3$ to $v'' = 0$ amounts to ~10^{-8} cm^3 s^{-1}. For $N_e = 10^{16}$–10^{17} cm^{-3} this yields characteristic times $\tau = 10^{-8}$–10^{-9} s. Therefore, the lag of the λ = 391.4 and 427.8 nm line glow peaks relative to the laser pulse is hard to explain by the e–V process. It is pertinent to note that Ref. [17] is the only paper which discussed the e–V process. Furthermore, the calculations of Ref. [17] were performed assuming Maxwellian electron velocity distribution. In our case, this condition may break down for a time period of tens of picoseconds after the action of a laser pulse.

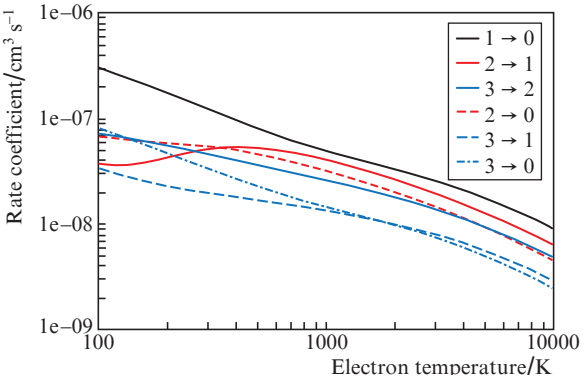

Figure 12. Maxwellian isotropic rate coefficient for the vibrational quenching of N_2^+ ions as a function of electron temperature.

The $B^2\Sigma_u^+$ ($v' = 3$) state of N_2^+ may also be populated due to the multiphoton ionisation of the N_2 molecule, as noted earlier. However, this is a low-probability process: according to the Frank–Condon principle, a higher probability is inherent in the transitions between these states without a change of the vibrational quantum number $v'' - v' = 0-0, 1-1, 2-2, 3-3$.

Electron impact is another way of excitation of the $B^2\Sigma_u^+$ ($v' = 0$) from the $X^2\Sigma_g^+$ ($v'' = 0$) state [18, 19]. This transition cross section σ was experimentally measured and theoretically calculated in Ref. [20]. This cross section peaks for an electron energy of 3.5 eV to range up to $\sim 3 \times 10^{-16}$ cm^2. It is well known that the rate coefficient k of the process may be estimated in terms of the cross section as $k = \sigma\langle v\rangle$, where $\langle v\rangle$ is the average electron velocity. In Ref. [18], the electron energy distribution function was calculated for the filament plasma in relation to the polarisation of pump radiation. For a linear polarisation, the distribution function exhibits a maximum about 0.5 eV, but a significant fraction of electrons has an energy of 3.5–4 eV, which is sufficient for exciting the transition under discussion. For these energies the electron velocity amounts to 1.2×10^8 cm s^{-1}, so that $k = 3 \times 10^{-16} \times 1.2 \times 10^8 = 3.6 \times 10^{-8}$ cm^3 s^{-1}. If the density of this fraction of electrons is equal to 5×10^{16} cm^{-3}, the characteristic excitation time $\tau = (3.6 \times 10^{-8} \times 5 \times 10^{16})^{-1} = 500$ ps. Consequently, the $B^2\Sigma_u^+$ ($v' = 0$) state excitation by electron impact also takes a long time.

Proceeding from the aforesaid, one may draw the following conclusions. The direct multiphoton mechanism of the $B^2\Sigma_u^+$ ($v' = 0$) state population is ruled out because of the lag of the peak of N_2^+ lines glow. The $X^2\Sigma_g^+$ ($v'' = 0$) – $B^2\Sigma_u^+$ ($v' = 0$) transition excitation by electron impact is a faster process than the e–V relaxation in the upper state $B^2\Sigma_u^+$. It is noteworthy that the lag of N_2^+ radiation peak was also observed in many other papers, both in the measurements of filament plasma luminescence [2–4] and of the superradiation generated in the filament [21, 22].

We analyse the duration of N_2^+ ion glow. As noted above, the upper electronic state may be quenched either by neutral particles or by electrons. Our estimates of the most probable processes in the plasma are collected in Table 1 assuming that $N_e = 10^{17}$ cm^{-3} and $T_e = 5000$ K.

Proceeding from the reaction rates presented, one may conclude that the main processes occur on a time scale of tens of picoseconds. Three-body reactions are the fastest ones. After being produced, the N_2^+ ions rapidly transform to N_4^+ by reaction 4. Competing with this process are reactions 1, 2, and 5: they all decrease the N_2^+ density significantly. However, it is noteworthy that reaction 4 becomes the dominant one if $N_e \approx 10^{16}$ cm^{-3}. This inference is experimentally borne out. Specifically, for a tight radiation focusing (NA > 0.1) and a high electron density ($N_e = 10^{18}$ cm^{-3}), molecular lines are not seen in the plasma glow, which is dominated by the lines of atoms and their ions. Conversely, for a weak focusing (NA < 0.03) the spectrum contains the lines of only N_2^+ an N_2. The emergent N_4^+ ions disappear in a very short time primarily due to reaction 8 with the production of N_2 in the state $C^3\Pi_u$, which is the upper state for the 2^+ system transitions. The rapid decay of the electron density observed in Fig. 9, is precisely what defines the two characteristic time intervals in the glow of N_2^+ and N_2: the moments of fast and slow decay.

Table 1. Parameters of quenching reactions.

Reaction number	Reaction and rate coefficient /cm^3 s^{-1}	Reference	Characteristic decay time/ps
	Reactions with participation of electrons		
1	$N_2^+ + e \to N + N$ $k = 1.34 \times 10^{-7}$	[23]	74
2	$N_2^+ + e + e \to N_2(X^1\Sigma_g^+) + e$ $k = 6.35 \times 10^{-25}$	[6]	157
3	$N_2^+ + e + N_2(X^1\Sigma_g^+) \to 2N_2(X^1\Sigma_g^+)$ $k = 5.29 \times 10^{-30}$	[23]	90000
	Reactions with participation of neutral particles		
4	$N_2^+ + 2N_2 \to N_4^+ + N_2$ $k = 1 \times 10^{-28}$	[23]	23
5	$N_2^+ + O_2 + N_2 \to NO^+ + N_2 + NO$	[1, 24]	56
6	$N_2^+ + O_2 \to NO^+ + N + O$ $k = 8 \times 10^{-10}$	[11]	220
7	$N_2^+ + N_2 \to N + N_3^+$ $k = 3 \times 10^{-10}$	[11, 23]	159
	Reactions of N_4^+ quenching		
8	$N_4^+ + e \to N_2(C^3\Pi_u) + N_2$ $k = 1.7 \times 10^{-6}$	[25]	6
9	$N_4^+ + e \to 2N_2(X^1\Sigma_g^+)$ $k = 4.9 \times 10^{-7}$	[6, 23]	20
10	$N_4^+ + N_2 \to N_2^+ + 2N_2(X^1\Sigma_g^+)$ $k = 8.3 \times 10^{-13}$	[23]	57000

The appearance of atomic or molecular lines depends primarily on the electron density and temperature. A low electron temperature ($T_e \leqslant 1000$ K) and (or) a high electron density ($N_e \geqslant 10^{17}$ cm^{-3}) determine a high rate of reactions 1–3, which quench the excited states of N_2^+. When the electrons manage to acquire sufficient energy (over 1 eV) from the field of the pump wave, their loss and disappearance of N_2^+ slows down, like the transfer of their acquired energy. This is precisely the scenario, in our view, observed in Ref. [1], in which the pump duration amounted to 500 fs.

5. Conclusions

We have measured the spectral, temporal and spatial dynamics of the plasma produced by a femtosecond radiation pulse in the air, with a time resolution of a few picoseconds. For given parameters of the laser beam, the plasma glow spectrum was shown to depend on the focusing conditions (numerical aperture NA). For high (over 0.1) NA, the spectrum is dominated by the lines of atoms and their ions, while for low (less

than 0.03) NA the spectrum shows the lines of only N_2^+ and N_2. For NA = 0.3, the onset of the glow of oxygen and nitrogen lines is delayed relative to the instant of plasma production by 80–90 ps. The production of molecular ions of nitrogen occurs due to its multiphoton ionisation and the subsequent finish excitation by electron impact. The delay of N_2^+ glow peak observed for NA = 0.03 is due to the finite rate of the electron excitation of the $B^2\Sigma_u^+$ ($v' = 0$) state and the high rate of its quenching in the course of ion collisions with neutral particles. The similarity of the leading edges of the ionic (λ = 391.4 nm) and molecular (357.7 nm) radiation intensity pulses as well as our analysis of the reaction rate coefficients count in favour of the mechanism of the $N_2(C^3\Pi_u)$ upper state production of the second positive system of nitrogen via the dissociative recombination of N_4^+. The short duration of molecular glow is due to a high rate of their quenching by electron impact. Under our conditions the duration of nitrogen ion glow pulse was equal to 18 ps, and that of molecular nitrogen to 27 ps at 1/e level of the peak. The existence of the second, slower stage in N_2 and N_2^+ glow is caused by a high rate of electron disappearance at the first points in time after irradiation. The diameter of the plasma channel remains invariable for 3 ns, while its glow intensity falls off by more than an order of magnitude. Therefore, the filament plasma recombines practically completely without expanding.

Acknowledgements. The authors express their gratitude to K.A. Sitnik for his assistance in the performance of experiments.

References

1. Martin F., Mawassi R., Vidal F., Gallimberti I., Comtois D., Pépin H., Kieffer J.C., Mercure H.P. *Appl. Spectrosc.*, **56**, 1444 (2002).
2. Xu H.L., Azarm A., Bernhardt J., Kamali Y., Chin S.L. *Chem. Phys.*, **360**, 171 (2009).
3. Ilyin A.A., Golik S.S., Shmirko K.A. *Spectrochimica Acta, Part B*, **112**, 16 (2015).
4. Lei M., Wu C., Liang Q., Zhang A., Li Y., Cheng Q., Wang S., Yang H., Gong Q., Jiang H. *Phys. B: At. Mol. Opt. Phys.*, **50**, 145101 (2017).
5. Bukin V.V., Vorob'ev N.S., Garnov S.V., Konov B.I., Lozovoi V.I., Malyutin A.A., Shchelev M.Ya., Yatskovskii I.S. *Quantum Electron.*, **36**, 638 (2006) [*Kvantovaya Elektron.*, **36**, 638 (2006)].
6. Aleksandrov N.L., Bodrov S.B., Tsarev M.V., Murzanev A.A., Sergeev Yu.A., Malkov Yu.A., Stepanov A.N. *Phys. Rev. E*, **94**, 013204 (2016).
7. Bernhardt J., Liu W., Théberge F., Xu H.L., Daigle J.F., Châteauneuf M., Dubois J., Chin S.L. *Opt. Commun.*, **281**, 1268 (2008).
8. Yang H., Zhang J., Li Y., Yang H., Zhang J., Li Y., Zhang J., Li Yu., Chen Z., Teng H., Wei Z., Sheng Z. *Phys. Rev. E*, **66**, 016406 (2002).
9. Papeer J., Botton M., Gordon D., Sprangle P., Zigler A., Henis Z. *New J. Phys.*, **16**, 123046 (2014).
10. Ivanov N.G., Losev V.F., Prokop'ev V.E., Sitnik K.A. *Opt. Commun.*, **387**, 322 (2017).
11. Valk F., Aints M., Paris P., Plank T., Maksimov J., Tamm A. *J. Phys. D: Appl. Phys.*, **43**, 385202 (2010).
12. Grien H. *Phys. Rev.*, **173**, 317 (1968).
13. Liu X.L., Lu X., Liu X., Xi T.T., Liu F., Ma J.L., Zhang J. *Opt. Express*, **18**, 26007 (2010).
14. Théberge F., Liu W., Simard P.T., Becker A., Chin S.L. *Phys. Rev. E*, **74**, 036406 (2006).
15. Ivanov N.G., Losev V.F. *Atm. Ocean. Opt.*, **30**, 331 (2017).
16. Madden R.P., Parr A.G. *Appl. Opt.*, **21**, 179 (1982).
17. Fifirig M. *Phys J. B: At. Mol. Opt. Phys.*, **48**, 085202 (2015).
18. Kartashov D., Ališauskas S., Pugžlys A., Shneider M., Baltuška A. *J. Phys. B: At. Mol. Opt. Phys.*, **48**, 094016 (2015).
19. Liu Y., Ding P., Lambert G., Houard A., Tikhonchuk V., Mysyrowicz A. *Phys. Rev. Lett.*, **115**, 133203 (2015).
20. Nagy O., Ballance C.P., Berrington K.A., Burke P.G., McLaughlin B.M. *J. Phys. B: At. Mol. Opt. Phys.*, **32**, L469 (1999).
21. Yao J., Xie H., Zeng B., Chu W., Li G., Ni J., Zhang H., Jing C., Zhang C., Xu H., Cheng Y., Xu Z. *Opt. Express*, **22**, 19005 (2014).
22. Zhong X., Miao Z., Zhang L., Liang Q., Lei M., Jiang H., Liu Y., Gong Q., Wu C. *Phys. Rev.*, **96**, 043422 (2017).
23. Vereshagin K.A., Smirnov V.V., Shachatov V.A. *J. Techn. Phys.*, **67**, 34 (1997).
24. Mitchell K.B. *Chem. Phys.*, **53**, 1795 (1970).
25. Fitaire M., Pointu A.M., Stathopoulos D., Vialle M. *Chem. Phys.*, **81**, 1753 (1984).